

NANO EXPRESS

Open Access



Characterization and Evaluation of Reverse Osmosis Membranes Modified with Ag₂O Nanoparticles to Improve Performance

Abdullah S. Al-Hobaib^{1*}, Khalid M. AL-Sheetan¹, Mohammed Rafi Shaik^{2*}, Naser M. Al-Andis² and M. S. Al-Suhybani¹

Abstract

The objective of this work was to prepare and characterize a new and highly efficient modified membrane by in situ interfacial polymerization on porous polysulfone supports. The process used *m*-phenylenediamine and trimesoyl chloride in hexane, incorporating silver oxide Ag₂O nanoparticles of varied concentrations from 0.001 to 0.1 wt%. Ag₂O nanoparticles were prepared at different sizes varying between 20 and 50 nm. The modified membranes were characterized by X-ray diffraction (XRD), scanning electron microscopy (SEM), energy-dispersive X-ray spectroscopy (EDX), atomic force microscopy (AFM), transmission electron microscopy (TEM), and contact angle measurement. The results showed a smooth membrane surface and average surface roughness from 31 to 74 nm. Moreover, hydrophilicity improved and the contact angle decreased to 41° at 0.009 wt% silver oxide. The performances of the developed membranes were investigated by measuring permeate fluxes and salt rejection capability by passing NaCl solutions (2000 ppm) through the membranes at 225 psi. The results showed that the flux increased from 26 to 40.5 L/m² h, while the salt rejection was high, at 99 %, with 0.003 wt% Ag₂O nanoparticles.

Keywords: Ag₂O nanoparticles; Interfacial polymerization; RO membrane; Modified membrane; Desalination

Background

Water purification technologies are attracting increasing attention, because of gradually increasing shortages of fresh water and lack of access to safe drinking water. Reverse osmosis (RO) is an important membrane technology for water purification through decontamination of industrial effluents and desalination of sea water. Recently, a number of workers have focused on developing high water flux membranes with low processing cost [1–8]. Several methods have already been developed for RO membrane fabrication including phase inversion [9] and interfacial polymerization (IP) [10]. However, concerted efforts are constantly applied to innovate new efficient supports [11], polymer types [12], and tailor polymer structures [13].

From ancient times, human beings have collected consumable fresh water from rivers, lakes, canals, ponds, and underground aquifers [14]. The sources of fresh water are depleted over time because of several reasons such as growth in population, industrialization, modernization of human societies, and enormous changes in climate. The sources of the fresh water are being contaminated significantly due to agricultural and industrial effluents flowing into lakes, canals, and rivers which are constantly leaking into underground water. These effluents contain many contaminants, such as metals, dyes, pesticides, fertilizers, and biologics, which are harmful to human consumption because of their toxicity [15, 16]. Therefore, human beings are always in search of fresh drinkable water sources for making it available to the consumer. In order to pursue this effort, many physical-chemical methods have been developed and adopted at different times. Some use chemical treatments to remove contaminants from polluted sweet water

* Correspondence: ahobaib@kacst.edu.sa; rafiskm@gmail.com

¹Nuclear Science Research Institute, King Abdulaziz City for Science and Technology (KACST), P.O. Box 6086, Riyadh 11442, Saudi Arabia

²Department of Chemistry, College of Science, King Saud University, P.O. Box. 2455, Riyadh 11451, Kingdom of Saudi Arabia

by adopting various techniques, while others use heat treatment to obtain fresh water through vaporization followed by condensation. These methods are not economically viable, are time consuming, and are environmentally hazardous and unfriendly.

The membrane composition and its subsequent surface chemistry accomplish its interaction with water, thus affecting its wettability. The membrane wettability can be calculated by assessing the contact angle between the membrane surface and a droplet of liquid. Hydrophilic membranes are characterized by the presence of active groups that have the ability to form hydrogen bonds with water and so these membranes have wettability. Generally, higher charge density on a membrane surface is accompanying with higher hydrophilicity of the membrane. Membrane surface morphology also has a considerable effect on flux, fouling as pore size, pore geometry, and pore size distribution particularly at the surface of the membrane [17].

Surface hydrophilicity augmented when the hydrophilic nanoparticles (NPs) were presented onto the surface of the membrane. Enriched water flux came from the hydrophilic membrane surface. Furthermore, water affinitive surface area improved if the nanoparticle had a higher degree of dispersion and also by increasing membrane hydrophilicity and reduce the cross-linking degree of polyamide thin-film composite membrane by competing with *m*-phenylenediamine (MPD), which ensued in a great enhancement of water flux. Further, the decrease of the cross-linking degree could also increase salt passage through the membrane [18, 19].

A great number of RO and nanofiltration (NF) membranes with good decontamination performances and permeate fluxes have been developed [20–23]. RO membranes have very high levels of rejection of inorganic solutes such as monovalent ions, hardness components (e.g., calcium, magnesium), and organic matters such as trihalomethane precursor, pesticides, and deodorants at operating pressures of approximately 0.5–6.0 MPa [24].

An RO membrane is composed of three layers: a bottom layer made of unwoven polyester cloth of thickness 100–200 μm to support the entire membrane, a middle layer consisting of polysulfone (PSF) or polyethersulfone (PES) of thickness 30–50 μm , and a top layer of polyamide (PA) or polyetherimide (PEI), supported by PSF or PES, of average thickness 100–200 nm, which is used to separate solutes from feed water. A PA membrane is prepared on the surface of the middle layer by interfacial polymerization between a diamine moiety of 1,3-phenylenediamine (MPD) in the water phase and an acid chloride moiety of 1,3,5-benzenetricarbonyl trichloride (TMC) in the nonpolar organic phase. An industrial product named FT-30 is one such RO membrane, which has a high level of salt rejection of more than 99 % and

fluxes of more than $1 \text{ m}^3/(\text{m}^2/\text{day})$ for 2000 ppm NaCl at 1.55 MPa [25]. Thus, many types of RO membranes have been developed.

Kamada et al. developed polyamide RO membranes with controlled surface morphology by interfacial polymerization of water-soaked MPD with TMC in an organic nonpolar hexane medium on polysulfone ultrafiltration supports [26].

Biofouling and virus penetration are two significant obstacles in water treatment using membrane filtration [27], because both reduce membrane permeability, increase energy costs, and decrease the lifetime of membranes. To effectively remove viruses, nanofiltration or reverse osmosis should be used with low-pressure membranes having anti-biofouling and antiviral properties. The antibacterial properties of silver are well known, and silver nanoparticles (nano-Ag) are now incorporated into polymer membranes, including RO membranes, as well as in a wide variety of consumer products for microbial control [27].

In this study, nano- Ag_2O was incorporated into RO membranes. Nanosilver oxide incorporation also increases membrane hydrophilicity and reduces the potential for other types of membrane fouling. The objectives of this paper were to prepare and characterize new and highly efficient modified polyamide (PA) membranes incorporating silver oxide (Ag_2O) nanoparticles. Ag_2O nanoparticles were prepared at different sizes, varying between 20 and 50 nm.

Methods

Materials

The materials and chemicals which were used in this study are of analytical grade as demonstrated in the following: polysulfone supports (PS-20) were purchased from Sepro, USA; *n*-hexane (99 %) was purchased from Oxford Laboratory, India; *m*-phenylenediamine (99 %) (MPD), 1,3,5-benzenetricarbonyl trichloride (TMC), silver nitrate, sodium oleate, triethylene glycol, and *n*-dodecane (99 %) were purchased from Sigma-Aldrich, USA; *n*-cyclohexane, *n*-heptane, and sodium carbonate anhydrous (99 %) were purchased from Scharlau, Spain; ammonium nitrate was purchased from Avonchem Limited, UK; and ultrapure deionized (DI) water was purchased from a Millipore Milli-Q system which was used in all experiments.

Preparation of Ag_2O Nanoparticles

Ag_2O nanoparticles were prepared by the method as follows: Equimolar quantity of silver nitrate 4.61 g (0.0271 mol) was reacted with 8.25 g (0.0271 mol) sodium oleate to yield silver oleate. The silver oleate thus obtained was added to triethylene glycol and heated to reflux temperature while stirring continuously for about

2 h. The reaction mixture was then centrifuged for 10 min and the supernatant was discarded and dried in an oven at 250 °C for 3 h to a powder, which was finely ground to obtain silver oxide nanoparticles [28].

Preparation of Polyamide Membranes

Polyamide thin-film composite membranes were prepared by immersing a commercial polysulfone product support (PS-20) in an aqueous solution of MPD (2 v/v%) for 2 min and then the excess MPD solution was removed by pressing the membrane under a rubber roller. The membrane was then immersed in 0.1 % of a TMC and hexane (99 %) solution for 1 min, rinsed with 0.2 % Na₂CO₃, washed with DI water, and finally stored in a refrigerator ≈4 °C in DI water prior to use.

Synthesis of Polyamide/Silver Oxide Nanocomposite Membranes

The silver oxide-polyamide nanocomposite membranes were synthesized similarly to thin-film composite (TFC) membranes, except that silver oxide nanoparticles were added in the 0.001–0.1 w/v% TMC in *n*-hexane solution beforehand. Various amounts of Ag₂O nanoparticles were dispersed in TMC-*n*-hexane solution by ultrasonication for 60 min at 20 °C. The resultant solution was immediately used for interfacial polymerization (IP) with MPD-soaked PS supports to form the thin-film nanocomposite (TFN) membranes.

Characterization

Scanning Electron Microscopy (SEM)

The morphology and microstructure of the as-synthesized nanocomposite membrane was examined by scanning electron microscope (SEM; FEI Nova-Nano SEM-600, The Netherlands).

Atomic Force Microscopy (AFM)

The AFM device was a nanosurf scanning probe-optical microscope (Bruker Corporation). Atomic force microscopy was used to analyze the surface morphology and roughness of the prepared membranes. Small squares of the prepared membranes (approximately 1 cm²) were cut and glued on a glass substrate for the analysis.

Goniometer

Contact angle analysis was performed using a Ramé-Hart Model 250 Standard Goniometer/Tensiometer with drop image advanced software (Ramé-Hart Instrument Co., Succasunna, NJ). A water droplet was placed on a dry, flat homogeneous membrane surface, and the contact angle between the water and membrane was measured until no further change was observed. The average contact angle for distilled water was determined in a

series of eight measurements for each of the different membrane surfaces.

Cross-Flow (Flux and Salt Rejection)

The performances of the prepared membranes were analyzed through a cross-flow system (CF042SS316 Cell, Sterlitech Corp., USA). The active membrane area in this system was 42 cm². The feed water temperature was 25 °C with pH adjusted between 6 and 7, for a 2000 ppm NaCl concentration and a feed flow rate of 1 gallon per minute (gpm). The filtration was carried out at a transmembrane pressure of 225 psi. All measurements of the water flux and salt rejection were measured after 30 min of water filtration experiments to ensure steady-state operation had been reached. A schematic of the cross-flow filtration system is shown in Fig. 1.

The flux was calculated using the following equation [29].

$$J = \left(\frac{1}{A}\right) \frac{dV_p}{dt} \quad (1)$$

where J is the water flux (L/m² h), V_p is the permeate volume (L), A is the membrane area (m²), and t is the treatment time (h). The salt rejection (R) was calculated using the following equation:

$$R = \left(1 - \frac{C_p}{C_f}\right) * 100 \quad (2)$$

where C_p and C_f are the salt concentrations in the permeate and feed streams, respectively.

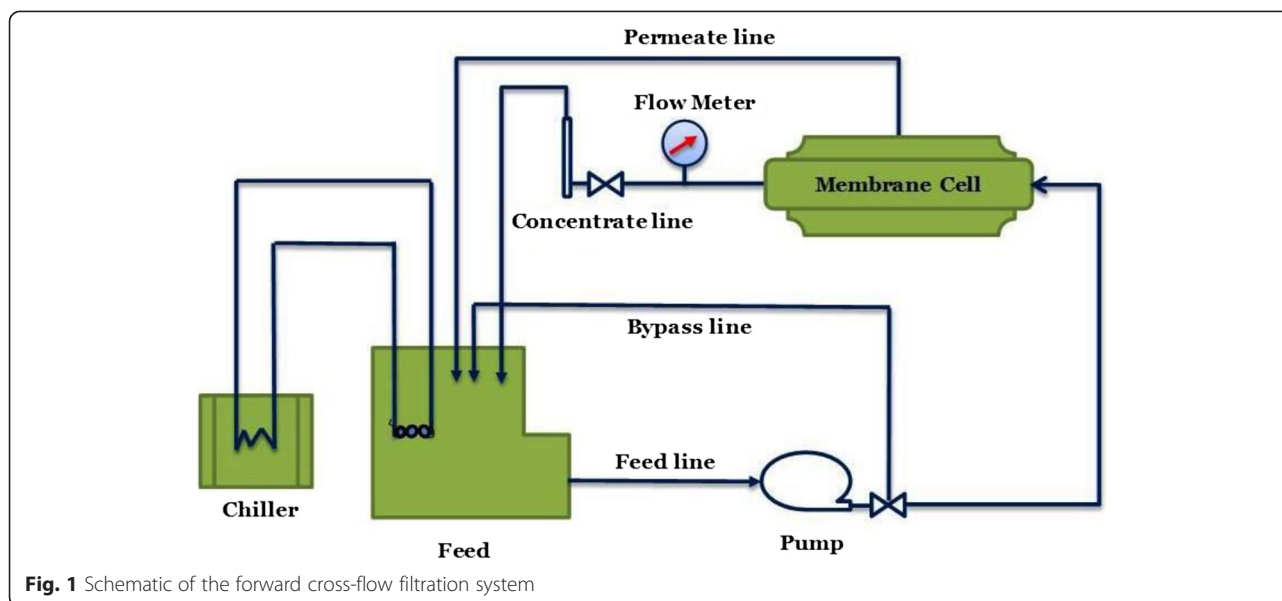
Results and Discussion

The synthesized silver oxide nanoparticles were characterized by SEM, transmission electron microscopy (TEM), energy-dispersive spectroscopy (EDX), and X-ray diffraction (XRD) as follows.

The size and surface morphology of Ag₂O nanoparticles were determined by SEM, as shown in Fig. 2b, and the size of silver nanoparticles was estimated, in the form of nanocrystallites. EDX carried out during the SEM analysis conformed to the characteristic peaks of Ag, as shown in Fig. 2a.

TEM analysis of Ag₂O nanoparticles was also carried out to estimate the size of silver nanoparticles. Particle size was estimated to be in the range of 18 to 50 nm, confirming the results already estimated by SEM and EDX. TEM images are shown in Fig. 3.

Typical XRD spectra of the silver oxide nanoparticle powder carried out after thermal treatment are shown in Fig. 4. Five pronounced diffraction peaks were observed and that resemble the characteristics of Ag₂O nanoparticles. Those five pronounced diffractogram peaks were found at 37.40° (111), 44.10° (200), 63.90° (220), 75.90° (311), and 80.90° (222). The average grain size was

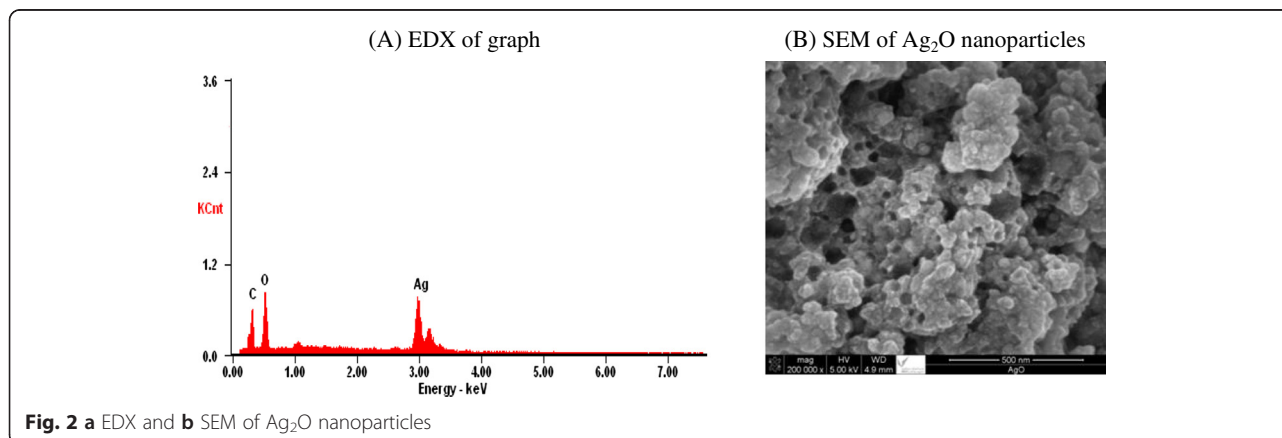


calculated using the Debye-Scherrer equation ($G = 0.9\lambda / \beta \cos\theta$), where λ is the X-ray wavelength (Cu, 1.5418 Å), θ is the maximum of the Bragg diffraction peak, and β is the full width at half maximum. After a correction for instrumental broadening, the average value obtained for the crystallites was 45 nm [30].

The TFC membrane layer was found to be coated onto the PS support base during the interfacial polymerization (IP) reaction process between MPD and TMC, leading to the formation of a leaf-like morphology. SEM and EDX analysis was used to determine such morphology as well as the size of silver nanoparticles in the membranes. EDX spectra and SEM images of the reference TFC membrane are shown in Fig. 5a, b, respectively. Similarly, EDX spectra and SEM images of polymer membranes containing silver nanoparticles are shown in Fig. 5c, d, respectively. It was observed that

impregnation of Ag_2O nanoparticles in the polymer matrix does not affect the overall morphology of TFC membranes containing silver nanoparticles, even when the wt% range of Ag_2O nanoparticles was increased to 0.02 wt% (Fig. 5f). However, partial aggregation of Ag_2O nanoparticles was observed in the polymer matrix. The difference between the images clearly indicates the presence of Ag_2O nanoparticles. This was further confirmed by EDX quantitative analysis, which clearly shows the presence of carbon, oxygen, and silver peaks as component elements. In comparison, a TFC reference membrane exhibited an ascendant and broadened ridge-valley structure, suggesting variation in surface roughness of TFC membranes under different nano- Ag_2O loadings.

AFM analysis was carried out to further determine the morphology and roughness of the membrane surface after incorporation of silver oxide nanoparticles into the



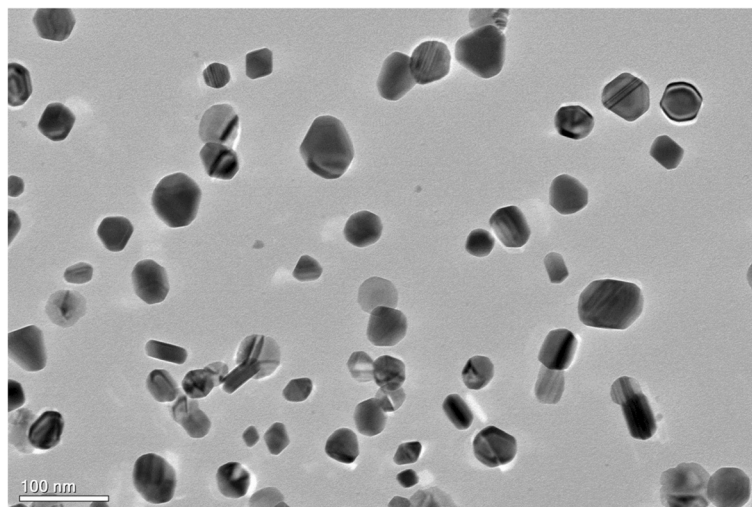


Fig. 3 TEM of Ag_2O nanoparticles

polymer membranes. AFM measurements of membranes containing different contents of silver oxide nanoparticles and are shown in Fig. 6. It can be observed that the roughness (R_a) values increased with increasing silver oxide content in the polymer membranes. TFC membranes with 0.02 wt% silver showed the highest surface roughness (i.e., $R_a = 74$ nm), compared with that of a TFC reference membrane without silver content ($R_a = 31$ nm). This difference is presumed to be caused by the leaf-like shape as well as by the aggregation of Ag_2O nanoparticles present in the membrane surface. The surface comprised continuous ridge and valley structures, confirming previous results obtained by other researchers [16, 20–22].

Membranes containing different amounts of silver oxide nanoparticles were subjected to contact angle

measurements to evaluate the hydrophilic and hydrophobic characteristics of the membranes; during contact angle measurements, reproducible standard deviation (SD) was taken into account with the ultimate aim of determining water permeate flux ability during the salt rejection process for underground water. An acceptable reproducible standard deviation was taken into account during the measurements. Contact angles, as measured with different PA membranes containing various amounts (wt%) of Ag_2O nanoparticles, are presented in Fig. 7.

It can be observed that contact angle significantly decreased with increased silver oxide content in the membranes. For example, the presence of a silver content of 0.003 wt% in the membrane dropped the contact angle from $94^\circ \pm 1.8^\circ$ to $45^\circ \pm 0.7^\circ$. Contact angles of the

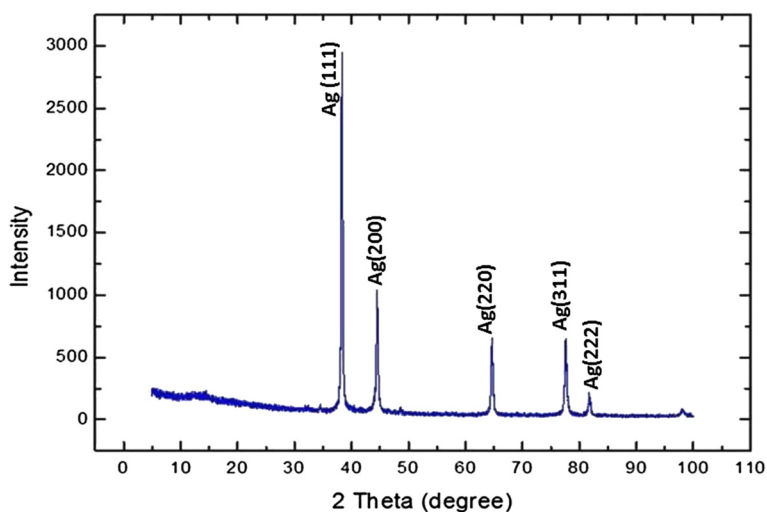
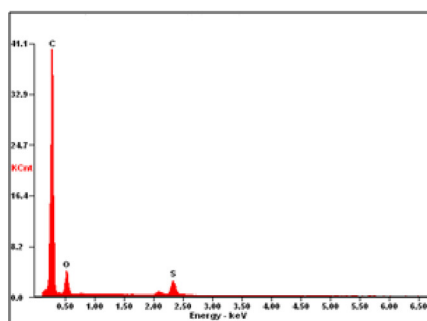
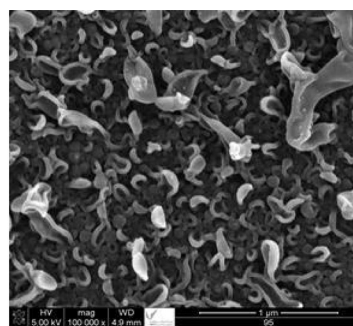


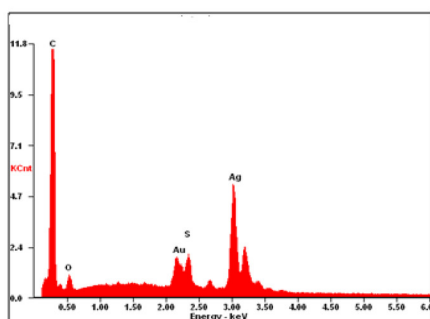
Fig. 4 XRD patterns of Ag_2O nanoparticles



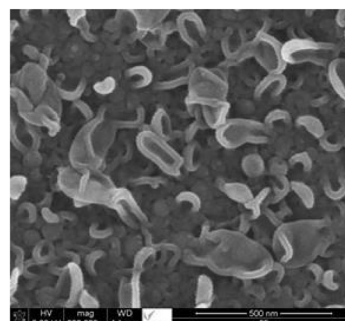
(A) EDX of TFC reference



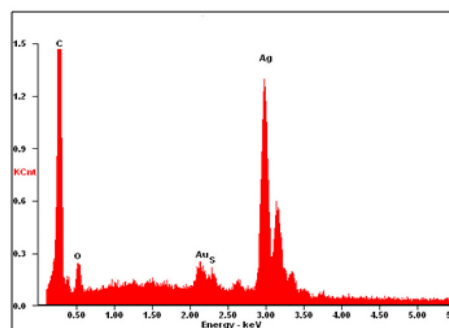
(B) SEM of TFC reference



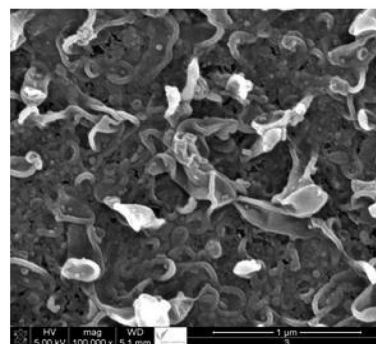
(C) EDX of modified membrane (0.003 wt%)



(D) SEM of modified membrane (0.003 wt%)



(E) EDX of modified membrane (0.02 wt%)



(F) SEM of modified membrane (0.02 wt%)

Fig. 5 SEM images and EDX of TFC reference membranes and membranes modified with Ag_2O nanoparticles. EDX (a) and SEM (b) of TFC reference. EDX (c) and SEM (d) of modified membrane (0.003 wt%). EDX (e) and SEM (f) of modified membrane (0.02 wt%)

membranes did not change/decrease markedly above 0.01 wt% silver loading. Additionally, the hydrophilicity did not change significantly, despite the increasing content of Ag_2O nanoparticles. Our results are in agreement with those obtained by other researchers [31]. It is known that there is a strong correlation between the geometry/stereochemistry of water at the solid-liquid interface and the hydrophilicity of the solid surface [32, 33]. Rearrangement of interfacial water molecules can increase hydrophilicity, thus improving water's ability to form hydrogen bonds and, in turn, producing stronger interactions between water and the solid phase in the polymer matrix, i.e., the TFC surface.

The remarkable decrease in contact angle in the presence of embedded silver oxide nanoparticles can be explained as follows:

1. A large amount of embedded spherical Ag_2O nanoparticles could have been exposed on the membrane surface. The hydrophilic nature of the silver nanoparticles would increase the hydrophilic character of the membrane surface and would also help water molecules to adhere to the Ag_2O nanoparticles, through capillary effects [34]. This is consistent with the result of Jeong et al. [35], who observed that the contact angle of membrane

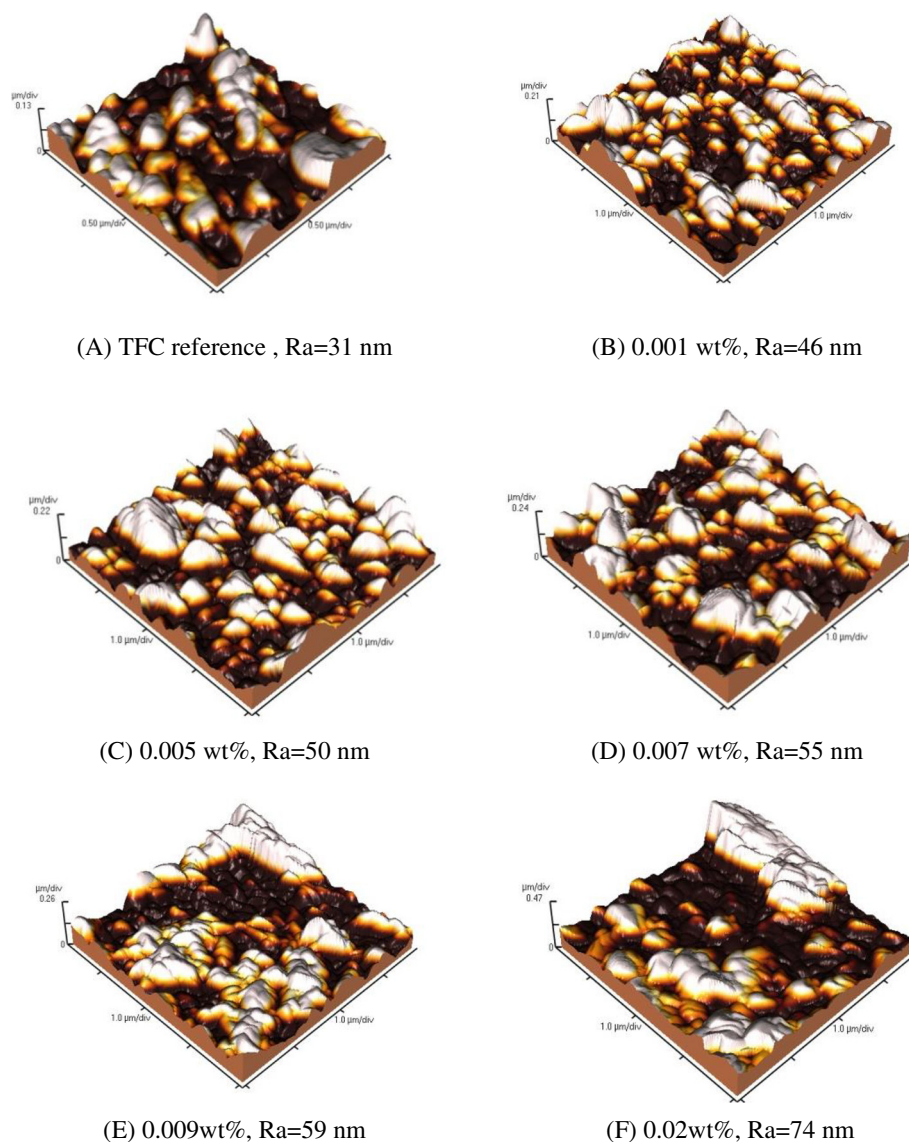


Fig. 6 AFM images of membranes modified with silver oxide nanoparticles. **a** TFC reference, Ra = 31 nm. **b** 0.001 wt%, Ra = 46 nm. **c** 0.005 wt%, Ra = 50 nm. **d** 0.007 wt%, Ra = 55 nm. **e** 0.009 wt%, Ra = 59 nm. **f** 0.02 wt%, Ra = 74 nm

surface decreased with increased zeolite content and attributed this to the super-hydrophilic property of the zeolite.

- Second, silver oxide nanoparticles may hydrate and release heat when contacting with MPD aqueous solution [36]. This process may affect the IP reaction between MPD and TMC and, subsequently, may change the matrix of the PS support. If a large number of acyl chloride groups of TMC remained on the membrane surface without reacting with the amine groups of MPD, the hydrolysis of acyl chloride could generate carboxylic acid functional groups, which may lead to increased hydrophilicity

[37]. It is known that the hydrophilic nature of Ag₂O nanoparticles can significantly improve the overall hydrophilicity of membranes, thereby creating favorable conditions for improved water flux and antifouling. It is well understood that the morphological structure and the hydrophilicity of the membrane are the two main factors that govern the filtration properties of membranes and those of TFC membranes [38].

Polymer membranes containing various amounts of Ag₂O nanoparticles were used to carry out a filtration process at 25 °C, using the cross-flow method. The

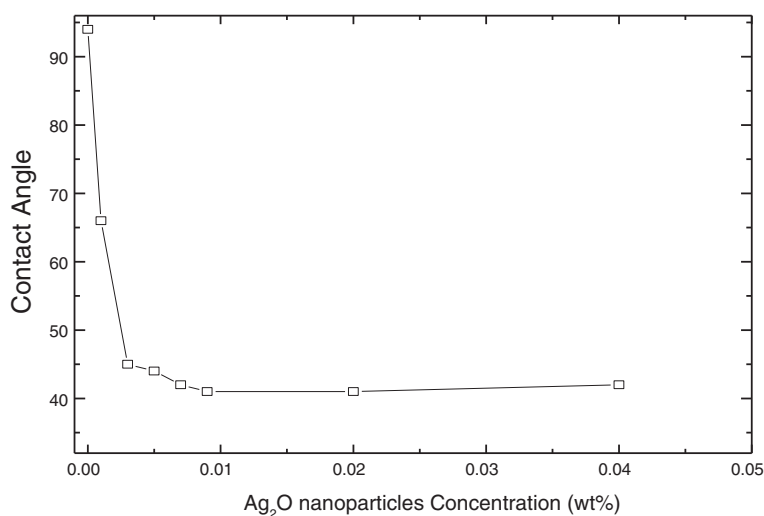


Fig. 7 Contact angles of PA membranes containing different amounts of silver nanoparticles

results of water permeate fluxes and salt rejections for all membranes are presented in Fig. 8.

The maximum of the hybrid membranes' water fluxes is greater than that of the TFC membranes ($25 \text{ L/m}^2 \text{ h} \pm 2.3$), where ± 2.3 is the standard deviation of three measurements which was used to estimate the uncertainty of these measurements. The quantity of Ag₂O nanoparticles was increased, and then the membrane water flux correspondingly increased up to a peak value at 0.003 wt% ($40.43 \text{ L/m}^2 \text{ h} \pm 3.0$) and then started to decrease. The peak value of water flux displays an enhancement of 160 % over that of the TFC reference membrane. On the

other side, the salt rejection of both thin-film composite (TFC) and thin-film nanocomposite (TFN) membranes was established to be $98 \% \pm 0.7$ and $99 \% \pm 0.1$, respectively. The SD was measured for three measurements in each case. Consequently, the standard deviation of salt rejection for TFN was within 2 %. It is postulated that the improved water permeability may be ascribed to the nanometer pores in the silver oxide nanoparticles. On the other hand, the silver oxide nanoparticles may interrupt the interfacial polymerization method to amend the active layer permeability. Furthermore, the increased membrane surface roughness might relatively explain such flux

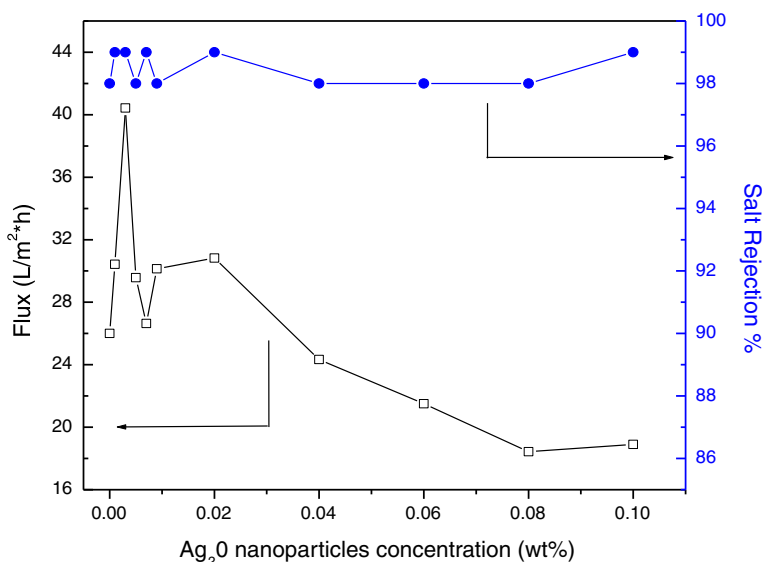


Fig. 8 Water permeate fluxes and salt rejections of modified membranes containing various amounts of Ag₂O nanoparticles

Table 1 Summary of membrane characteristics of present study

MPD	TMC	Additives	Conc. %	Salt rejection %	Flux (L/m ² h)
Constant at 2 %	Constant at 0.1 %	Ag ₂ O	0.001	99 ± 0.1	30.43 ± 2.1
			0.003	99 ± 0.1	40.43 ± 3.0
			0.005	98 ± 0.3	29.57 ± 1.9
			0.007	99 ± 0.1	26.64 ± 2.2
			0.009	98 ± 0.2	30.14 ± 2.1
			0.02	99 ± 0.1	30.83 ± 2.9
			0.04	94 ± 0.7	24.33 ± 1.7
			0.06	98 ± 0.2	21.50 ± 2.2
			0.08	97 ± 0.9	15.43 ± 2.9
			0.10	99 ± 0.1	18.90 ± 2.1

n-Hexane (99 %), pressure (225 psi), and rate (1 gpm). The experimental data were reported as the average value of at least three repeated measurements in tests, error bars based on measurements of three coupons

enrichment. On the other hand, a high silver oxide loading may help to develop a comparatively thicker rejection polyamide layer, which decreased the water permeability and improved salt rejection. The transport properties of the membranes prepared in this study are listed in Table 1.

Both permeate flux and salt rejection ability depend on the polyamide layer density, which is related to cross-linking density [39]. The polymer density across the barrier layer is not uniform [40]. The core layer (near the original MPD/TMC interface) is the most dense region, and the polymer density decreases gradually as the polymer grows further into the organic phase [41, 42]. In many applications of interfacial polymerization using MPD and TMC, the initial amine concentration is much higher than the acyl chloride concentration. Whether

the amine concentration is decreased or the acyl chloride concentration is increased, this results in a more dense polyamide layer, compared with those prepared using higher amine/acid chloride molar ratios [43]. An increase in density or in thickness of the MPD/TMC barrier layer would increase the mass transfer resistance of the resulting membrane, thereby reducing permeate flux. Thus, varying the initial concentration of monomers can influence the membrane's water and salt transport properties.

TFC-modified membranes were prepared by varying the concentrations of MPD and TMC and keeping the mass of added Ag₂O nanoparticles at 0.003 wt%. Figure 9 shows the influence of varying the MPD concentration on permeate flux and salt passage. Similarly, Fig. 10 presents the influence of changing the TMC concentration on flux and salt rejection.

Salt passage was found to be relatively insensitive to changes in MPD concentration. This suggests the formation of defect-free membranes in all cases. Maximum permeate flux was exhibited near 2 w/v% MPD. As the MPD concentration was increased, the driving force for MPD diffusion into the organic phase increased. Increased MPD concentration could, therefore, increase the barrier layer thickness and, thus, causes a lower permeate flux. As MPD concentration decreased, layer thickness was expected to decrease, which would tend to increase flux, but the resulting layer was also expected to become more dense as the molar ratio of amine/acyl chloride approached unity, which would lower flux [41, 44].

Figure 10 illustrates the influence of TMC concentration in the organic phase on permeate flux and salt passage at a constant MPD concentration of 2 w/v% in the

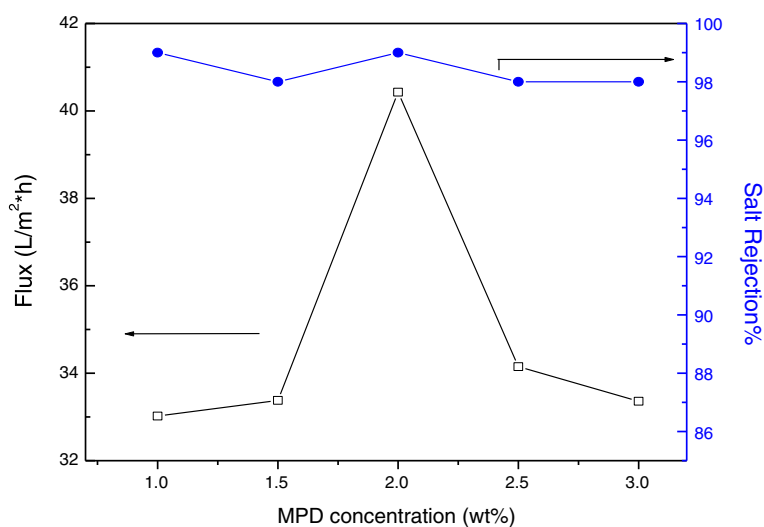


Fig. 9 Water permeate flux and salt rejection of modified membranes containing fixed amounts of Ag₂O nanoparticles at 0.003 wt% and TMC at 0.1 w/v%

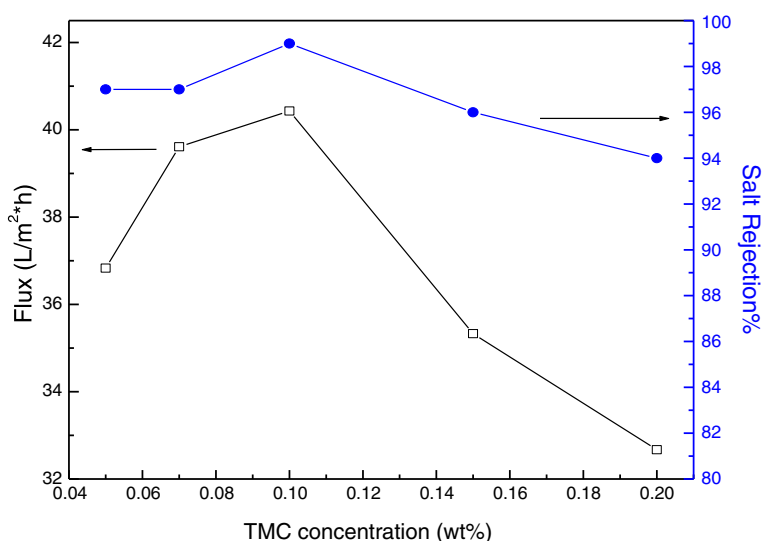


Fig. 10 Water permeate flux and salt rejection of modified membranes containing fixed amounts of Ag_2O nanoparticles at 0.003 wt% and MPD at 2 w/v%

aqueous phase, which was observed in Fig. 9 to be near the optimum flux value. Interfacial polymerization is typically MPD diffusion-controlled during growth of the polyamide layer. If TMC concentration is increased, the amine/acyl chloride molar ratio will decrease. This will, in turn, increase film density, causing a lower permeate flux [41, 44]. However, a decrease in permeate flux was also observed at the lowest TMC concentration of <0.1 %. Thus, the interfacial polymerization reaction is also reported to be TMC diffusion-limited [45]. A low concentration of acyl chloride groups in the reaction zone

may allow the polyamide film to grow thicker, which would decrease flux [39].

All the above experiments were carried out in a hexane medium. To investigate the influence of solvents on permeate flux and salt rejection, hexane was replaced with *n*-cyclohexane, *n*-heptane, and *n*-dodecane solvents. Figures 11 and 12 show the results for flux and salt rejection, respectively, and are in the order of *n*-dodecane > *n*-heptane > *n*-cyclohexane > *n*-hexane. However, the change in salt rejection with all these solvents was found to be within 2 % (Fig. 12).

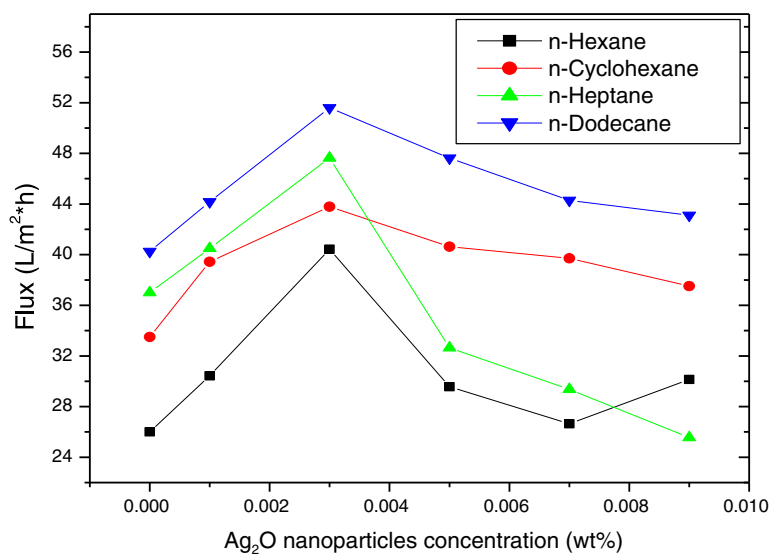


Fig. 11 Water flux with different solvents

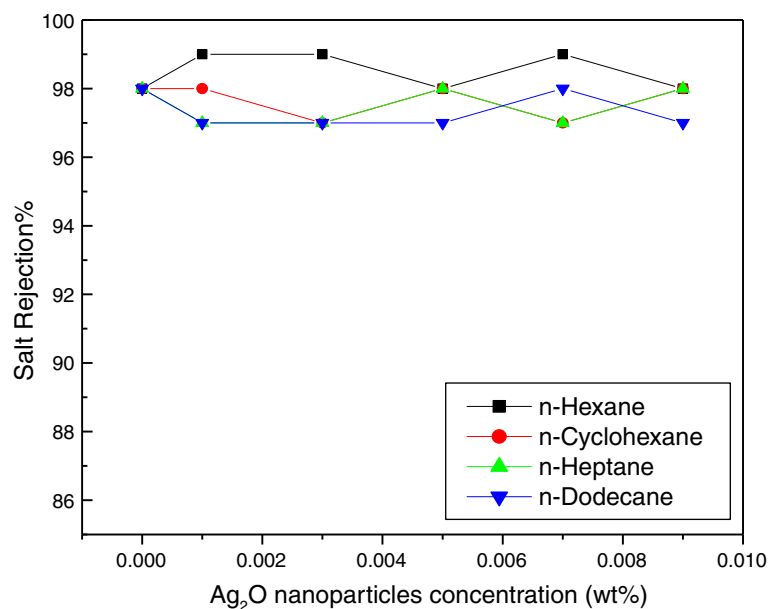


Fig. 12 Salt rejection with different solvents

There are many literature reports regarding the performance of interfacial polymerized commercial polyamide TFC membranes and of aromatic polyamide and TFC desalination membranes based on MPD and TMC [46–54]. The transport properties of the membranes prepared in this study were found comparable to those of the membranes listed in Table 2.

Conclusions

Silver oxide nanoparticles were embedded into the polyamide membrane through an interfacial polymerization process between MPD and TMC. EDX and SEM confirmed the formation of polyamide membranes embedded with silver oxide nanoparticles. EDX quantitative analysis confirmed the presence of silver oxide in

Table 2 Summary of membrane characteristics from previous studies

Nanoparticle type	Method	Modified membrane properties	Salt rejection	Flux (L/m ² h)	Ref.
MgTiO ₃ nanoparticles	IP (MPD/TMC) MgTiO ₃ in TMC/hexane	Enhanced surface hydrophilicity, increase roughness	98	45	[46]
Zeolite nanoparticles	IP (MPD/TMC) NaA in TMC/hexane	Smoother, hydrophilic, and negatively charged surfaces	93	40.2	[47]
Silica nanoparticles	IP (MPD/TMC) Silica in MPD/water	Silica particle interacting well with the polyamide	91	27.2	[48]
Silica nanoparticles	IP (MPD/TMC) Silica in MPD/water	Tunable pore radius and higher thermal stability	71.7	40.8	[49]
Silver nanoparticles	IP (MPD/BTC) Silver in BTC	Higher anti-biofouling effect	97	94	[50]
TiO ₂ nanoparticles	The neat TFC membrane was dipped in the transparent TiO ₂ colloidal solution	Higher photocatalytic bactericidal efficiency under UV light	96.6	24.5	[51]
TiO ₂ nanoparticles	IP (MPD/TMC) TiO ₂ in TMC and HCFC	Enhanced surface hydrophilicity	95	9.1	[52]
Zeolite nanoparticles	IP (MPD/TMC) NaY in TMC/hexane	Increase roughness and contact angle	90.5	43.7	[53]
Al ₂ O ₃ nanoparticles	IP (MPD/TMC) Al ₂ O ₃ in TMC/hexane	Enhanced surface hydrophilicity	88	5	[54]

polyamide components. Water flux and salt rejection performances revealed that the nanocomposite membrane was superior to the native (unmodified) membrane. Moreover, permeate flux was improved (from 26 to 40.5 L/m² h), while salt rejection performances remained within 2 %.

Competing Interests

The authors declare that they have no competing interests.

Authors' Contributions

ASAI-H and MRS designed the project and helped to draft the manuscript. KMAL-S carried out the experimental part with synthesis of nanocomposite membrane and their characterization. MSAI-S carried out some of the characterizations and interpretation of the results. ASAI-H and NMAI-A provided scientific guidance for successful completion of the project and also helped to draft the manuscript. All authors read and approved the final manuscript.

Acknowledgements

The authors are grateful to the King Abdulaziz City for Science and Technology, Riyadh, Saudi Arabia, for the financial support of this work and the facilities in its labs. This work was supported by King Saud University, Deanship of Scientific Research, College of Science, Research Center.

Received: 13 July 2015 Accepted: 17 September 2015

Published online: 29 September 2015

References

- Kim SH, Kwak S-Y, Sohn B-H, Park TH. Design of TiO₂ nanoparticle self-assembled aromatic polyamide thin-film-composite (TFC) membrane as an approach to solve biofouling problem. *J Membr Sci.* 2003;211(1):157–65.
- Ghosh AK, Hoek EM. Impacts of support membrane structure and chemistry on polyamide–polysulfone interfacial composite membranes. *J Membr Sci.* 2009;336(1):140–8.
- Van Voorthuizen EM, Zwijnenburg A, Wessling M. Nutrient removal by NF and RO membranes in a decentralized sanitation system. *Water Res.* 2005;39(15):3657–67.
- Peng X, Jin J, Nakamura Y, Ohno T, Ichinose I. Ultrafast permeation of water through protein-based membranes. *Nat Nanotech.* 2009;4(6):353–7.
- Zhou M, Nemade PR, Lu X, Zeng X, Hatakeyama ES, Noble RD, et al. New type of membrane material for water desalination based on a cross-linked bicontinuous cubic lyotropic liquid crystal assembly. *J Am Chem Soc.* 2007;129(31):9574–5.
- Tsuru T. Inorganic porous membranes for liquid phase separation. *Sep Purif Rev.* 2001;30(2):191–220.
- AL-Sheetan KM, Shaik MR, Al-Hobaib AS, Alandis NM. Characterization and evaluation of the improved performance of modified reverse osmosis membranes by incorporation of various organic modifiers and SnO₂ nanoparticles. *J Nanomater.* 2015;Article ID 363175:1–11.
- Suk M, Raghunathan A, Aluru N. Fast reverse osmosis using boron nitride and carbon nanotubes. *Appl Phys Lett.* 2008;92(13):133120.
- Petersen RJ. Composite reverse osmosis and nanofiltration membranes. *J Membr Sci.* 1993;83(1):81–150.
- Rao AP, Desai N, Rangarajan R. Interfacially synthesized thin film composite RO membranes for seawater desalination. *J Membr Sci.* 1997;124(2):263–72.
- Yoon K, Hsiao BS, Chu B. High flux nanofiltration membranes based on interfacially polymerized polyamide barrier layer on polyacrylonitrile nanofibrous scaffolds. *J Membr Sci.* 2009;326(2):484–92.
- Li L, Zhang S, Zhang X. Preparation and characterization of poly(piperazineamide) composite nanofiltration membrane by interfacial polymerization of 3, 3', 5, 5'-biphenyl tetraacyl chloride and piperazine. *J Membr Sci.* 2009;335(1):133–9.
- Tarboush BJA, Rana D, Matsuura T, Arafat H, Narbaitz R. Preparation of thin-film-composite polyamide membranes for desalination using novel hydrophilic surface modifying macromolecules. *J Membr Sci.* 2008;325(1):166–75.
- Jenerette GD, Larsen L. A global perspective on changing sustainable urban water supplies. *Global Planet Change.* 2006;50(3):202–11.
- Kim I-C, Lee K-H. Dyeing process wastewater treatment using fouling resistant nanofiltration and reverse osmosis membranes. *Desalination.* 2006;192(1):246–51.
- Ju H, McCloskey BD, Sagle AC, Wu Y-H, Kusuma VA, Freeman BD. Crosslinked poly(ethylene oxide) fouling resistant coating materials for oil/water separation. *J Membr Sci.* 2008;307(2):260–7.
- Kim SG, Hyeon DH, Chun JH, Chun B-H, Kim SH. Nanocomposite poly(arylene ether sulfone) reverse osmosis membrane containing functional zeolite nanoparticles for seawater desalination. *J Membr Sci.* 2013;443:10–8.
- Dong H, Zhao L, Zhang L, Chen H, Gao C, Ho WW. High-flux reverse osmosis membranes incorporated with NaY zeolite nanoparticles for brackish water desalination. *J Membr Sci.* 2015;476:373–83.
- Zhao L, Ho WW. Novel reverse osmosis membranes incorporated with a hydrophilic additive for seawater desalination. *J Membr Sci.* 2014;455:44–54.
- Tang CY, Kwon Y-N, Leckie JO. Effect of membrane chemistry and coating layer on physicochemical properties of thin film composite polyamide RO and NF membranes. I. FTIR and XPS characterization of polyamide and coating layer chemistry. *Desalination.* 2009;242(1):149–67.
- Baker RW. *Membrane Technology*. Kirk-Othmer encyclopedia of Chemical technology. 2000; DOI: 10.1002/0471238961.1305130202011105.a01.
- Kurihara M, Hanakawa M. Mega-ton Water System: Japanese national research and development project on seawater desalination and wastewater reclamation. *Desalination.* 2013;308:131–7.
- Xie W, Geise GM, Freeman BD, Lee H-S, Byun G, McGrath JE. Polyamide interfacial composite membranes prepared from m-phenylene diamine, trimesoyl chloride and a new disulfonated diamine. *J Membr Sci.* 2012;403:152–61.
- Vrijenhoek EM, Hong S, Elimelech M. Influence of membrane surface properties on initial rate of colloidal fouling of reverse osmosis and nanofiltration membranes. *J Membr Sci.* 2001;188(1):115–28.
- Cadotte JE. Interfacially synthesized reverse osmosis membrane. Google Patents. 1981.
- Kamada T, Ohara T, Shintani T, Tsuru T. Optimizing the preparation of multi-layered polyamide membrane via the addition of a co-solvent. *J Membr Sci.* 2014;453:489–97.
- Zodrow K, Brunet L, Mahendra S, Li D, Zhang A, Li Q, et al. Polysulfone ultrafiltration membranes impregnated with silver nanoparticles show improved biofouling resistance and virus removal. *Water Res.* 2009;43(3):715–23.
- Siddiqui MRH, Adil S, Assal M, Ali R, Al-Warthan A. Synthesis and characterization of silver oxide and silver chloride nanoparticles with high thermal stability. *Asian J Chem.* 2013;25(6):3405–9.
- Lind ML, Eumine Suk D, Nguyen T-V, Hoek EM. Tailoring the structure of thin film nanocomposite membranes to achieve seawater RO membrane performance. *Environ Sci Technol.* 2010;44(21):8230–5.
- Khan M, Khan M, Adil SF, Tahir MN, Tremel W, Alkhatlan HZ, et al. Green synthesis of silver nanoparticles mediated by *Pulicaria glutinosa* extract. *Int J Nanomedicine.* 2013;8:1507–16.
- Yin J, Kim E-S, Yang J, Deng B. Fabrication of a novel thin-film nanocomposite (TFN) membrane containing MCM-41 silica nanoparticles (NPs) for water purification. *J Membr Sci.* 2012;423:238–46.
- Hurwitz G, Guillen GR, Hoek EM. Probing polyamide membrane surface charge, zeta potential, wettability, and hydrophilicity with contact angle measurements. *J Membr Sci.* 2010;349(1):349–57.
- Du Q, Freysz E, Shen YR. Surface vibrational spectroscopic studies of hydrogen bonding and hydrophobicity. *Science.* 1994;264(5160):826–8.
- Li J-H, Xu Y-Y, Zhu L-P, Wang J-H, Du C-H. Fabrication and characterization of a novel TiO₂ nanoparticle self-assembly membrane with improved fouling resistance. *J Membr Sci.* 2009;326(2):659–66.
- Jeong B-H, Hoek EM, Yan Y, Subramani A, Huang X, Hurwitz G, et al. Interfacial polymerization of thin film nanocomposites: a new concept for reverse osmosis membranes. *J Membr Sci.* 2007;294(1):1–7.
- Lind ML, Ghosh AK, Jawor A, Huang X, Hou W, Yang Y, et al. Influence of zeolite crystal size on zeolite-polyamide thin film nanocomposite membranes. *Langmuir.* 2009;25(17):10139–45.
- Kim C, Kim J, Roh I, Kim J. The changes of membrane performance with polyamide molecular structure in the reverse osmosis process. *J Membr Sci.* 2000;165(2):189–99.
- Wu H, Tang B, Wu P. Novel ultrafiltration membranes prepared from a multi-walled carbon nanotubes/polymer composite. *J Membr Sci.* 2010;362(1):374–83.

39. Song Y, Sun P, Henry LL, Sun B. Mechanisms of structure and performance controlled thin film composite membrane formation via interfacial polymerization process. *J Membr Sci.* 2005;251(1):67–79.
40. Mitchell GE, Mickols B, Hernandez-Cruz D, Hitchcock A. Unexpected new phase detected in FT30 type reverse osmosis membranes using scanning transmission X-ray microscopy. *Polymer.* 2011;52(18):3956–62.
41. Freger V. Nanoscale heterogeneity of polyamide membranes formed by interfacial polymerization. *Langmuir.* 2003;19(11):4791–7.
42. Pacheco FA, Pinnau I, Reinhard M, Leckie JO. Characterization of isolated polyamide thin films of RO and NF membranes using novel TEM techniques. *J Membr Sci.* 2010;358(1):51–9.
43. Berezkin AV, Khokhlov AR. Mathematical modeling of interfacial polycondensation. *J Polym Sci Part B: Polym Phys.* 2006;44(18):2698–724.
44. Freger V, Srebniak S. Mathematical model of charge and density distributions in interfacial polymerization of thin films. *J Appl Polym Sci.* 2003;88(5):1162–9.
45. Chai G-Y, Krantz WB. Formation and characterization of polyamide membranes via interfacial polymerization. *J Membr Sci.* 1994;93(2):175–92.
46. Al-Hobaib A, El Ghoul J, El Mir L. Fabrication of polyamide membrane reached by MgTiO₃ nanoparticles for ground water purification. *Desalin Water Treat.* 2015; 1–10. (ahead-of-print)
47. Domingues SH, Salvatierra RV, Oliveira MM, Zarbin AJ. Transparent and conductive thin films of graphene/polyaniline nanocomposites prepared through interfacial polymerization. *Chem Commun.* 2011;47(9):2592–4.
48. Singh PS, Aswal VK. Characterization of physical structure of silica nanoparticles encapsulated in polymeric structure of polyamide films. *J Colloid Interface Sci.* 2008;326(1):176–85.
49. Jadav GL, Singh PS. Synthesis of novel silica-polyamide nanocomposite membrane with enhanced properties. *J Membr Sci.* 2009;328(1):257–67.
50. Lee SY, Kim HJ, Patel R, Im SJ, Kim JH, Min BR. Silver nanoparticles immobilized on thin film composite polyamide membrane: characterization, nanofiltration, antifouling properties. *Polym Advan Technol.* 2007;18(7):562–8.
51. Kwak S-Y, Kim SH, Kim SS. Hybrid organic/inorganic reverse osmosis (RO) membrane for bactericidal anti-fouling. 1. Preparation and characterization of TiO₂ nanoparticle self-assembled aromatic polyamide thin-film-composite (TFC) membrane. *Environ Sci Technol.* 2001;35(11):2388–94.
52. Lee HS, Im SJ, Kim JH, Kim HJ, Kim JP, Min BR. Polyamide thin-film nanofiltration membranes containing TiO₂ nanoparticles. *Desalination.* 2008;219(1):48–56.
53. Ma N, Wei J, Liao R, Tang CY. Zeolite-polyamide thin film nanocomposite membranes: towards enhanced performance for forward osmosis. *J Membr Sci.* 2012;405:149–57.
54. Saleh TA, Gupta VK. Synthesis and characterization of alumina nano-particles polyamide membrane with enhanced flux rejection performance. *Sep Purif Technol.* 2012;89:245–51.

Submit your manuscript to a SpringerOpen[®] journal and benefit from:

- Convenient online submission
- Rigorous peer review
- Immediate publication on acceptance
- Open access: articles freely available online
- High visibility within the field
- Retaining the copyright to your article

Submit your next manuscript at ► springeropen.com
